Absorption Enhancement in Organic-Inorganic Halide Perovskite Films with Embedded Plasmonic Gold Nanoparticles

*S. Carretero-Palacios, M. E. Calvo, H. Míguez**

Multifunctional Optical Materials Group, Instituto de Ciencia de Materiales de Sevilla, Consejo Superior de Investigaciones Científicas−Universidad de Sevilla (US-CSIC), Américo Vespucio 49, 41092 Sevilla, Spain.

Corresponding Author

*h.miguez@csic.es

ABSTRACT

We report on the numerical analysis of solar absorption enhancement in organic-inorganic halide perovskite films embedding plasmonic gold nanoparticles. The effect of particle size and concentration is analyzed in realistic systems in which random particle location within the perovskite film and the eventual formation of dimers are also taken into account. We find a maximum integrated solar absorption enhancement of ~ 10% in perovskite films of 200 nm thickness, and ~ 6% in 300 nm films, with spheres of radii 60 nm and 90 nm, respectively, in volume concentrations of around 10% in both cases. We show that the presence of dimers boosts the absorption enhancement up to ~ 12% in the thinnest films considered. Absorption reinforcement arise from a double contribution of plasmonic near field and scattering effects, whose respective weight can be discriminated and evaluated from the simulations.

TOC GRAPHICS

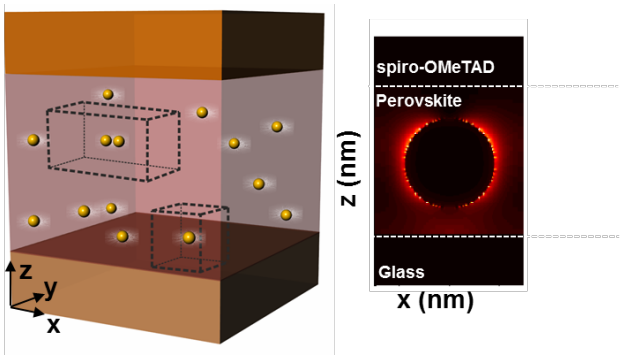

KEYWORDS Photovoltaics, Perovskite, Gold Nanoparticles, Optical Design.

1. INTRODUCTION

Since the emergence of organic-inorganic halide perovskite solar cells,[1,2] different synthetic approaches have been explored to improve their performance.[3,4] Efforts have been put in controlling the composition[5-7] or structural ordering[8] of perovskite films, as well as to provide the solar cells made out of them with other attractive properties apart from their high efficiency, such as flexibility[9], transparency[8] and color.[10] Also, motivated from the environmental issues related to the use of heavy metals, the viability of lead-free variants have been tested.[11,12]

From a different perspective, recent analysis of the optical response of these photovoltaic systems[13,14,15] have shown that light collection at long wavelengths ($\lambda \epsilon$ [650,800] nm) is not optimized, opening a new route to increase the performance of the device. Contrarily to what happened in other dye sensitized cells, in which the introduction of photonic crystals led to a significant increase of the short circuit photocurrent, [16-19], integrating dielectric mirrors inside perovskite solar cells cannot be used to improve light harvesting in any configuration, although it has been proven that this approach allows attaining a wide color pallet range, which makes the cells attractive for applications in building integrated photovoltaics.[20] In this regard, localized surface plasmon effects characteristic of metal nanoparticles might be used to enhance optical absorption at well-defined spectral ranges. In particular, gold nanoparticles (AuNPs) display localized plasmon resonances in the red part of the visible spectrum,[21] producing near- and far-optical field effects that give rise to intensity enhancement in the surroundings of the NP and strong scattering, respectively. Both phenomena can be tuned to match the spectral range of interest, forcing more light to be absorbed and therefore improving the perovskite cell performance. A few initial attempts exploring this possibility have already been reported. Different experimental approaches were taken based on silica coated gold spheres and gold-

silver alloy particle clusters of irregular or planar shapes.[22-24] In all cases, cell performance enhancements are observed, although the potential contribution of near field enhancement effects are largely diminished or excluded, as the metal particles are coated with a layer of silica, or not embedded within the active layer. In the first case, the improvement is attributed to a decrease of the exciton binding energy, which gives rise to enhanced free carrier generation, and not enlarged light absorption.[22]In the others, it is thought to be the result of multiple scattering[23] and faster charge transfer at the TiO_2-perovskite interface.[23]

Herein we present a detailed theoretical analysis of the effect of incorporating plasmonic gold nanoparticles on the optical absorption of organic-inorganic halide perovskite thin films. An increase light collection in the spectral range where the material absorbs less, which corresponds to the spectral range at which maximum number of solar photons impinge on the Earth surface, and plasmonic effects take place, is observed. On this basis, we perform systematic studies to optimize solar light absorption of such perovskite thin films with embedded gold nanoparticles. With this aim, we analyze plasmonic near field enhancement and scattering effects as a function of particle size, concentration, particle location and dimer formation, in order to account for all potential eventualities occurring during particle dispersion within the film and hence to determine design rules that maximize perovskite sunlight harvesting properties.

2. RESULTS AND DISCUSSION

Three-dimensional (3D) Finite-Difference Time-Domain (FDTD) simulations are performed using the software FDTD Solutions from Lumerical Solutions. A schematics of the systems here analyzed are shown in Figure 1, in which it can be seen that, in a first approximation, gold particles are considered to be dispersed in the middle of the perovskite film, at equal distances

from both surfaces. We consider a plane wave propagating along the z-direction and impinging on a perovskite slab of a certain thickness, L_z, containing a single gold nanoparticle (NP), having a semi-infinite glass substrate and a semi-infinite spiro-OMeTAD cover. We apply symmetry boundary conditions along the x and y directions, defining L_x and L_y sizes of the perovskite slab, respectively. The complex refractive index, $\tilde{n}_P(\omega) = n(\omega) + ik(\omega)$, of the $CH_3NH_3PbI_3$ perovskite here considered is extracted from experimental values tabulated in Ref.[20], which are provided in Figure S1 in the Supporting Information. Since it cannot be fitted to any available analytical model, single wavelength simulations are performed $\lambda \epsilon$ [400,800] nm. For the glass substrate we take $\tilde{n}_G(\omega) = 1.5$ and for the spiro-OMeTAD medium, $\tilde{n}_S(\omega) = 1.7$. The refractive index of gold, $\tilde{n}_{Au}(\omega)$, is obtained from Ref.[25].

Perovskite and gold absorptances are calculated independently through:

$$A_j = \omega\varepsilon_0 \int |E(x,y,z,\omega)|^2 n_j(\omega) k_j(\omega) dV_j$$

with ω the angular frequency, E the electric field vector, and j standing for either perovskite, P, or gold, Au. The integral is done over the corresponding perovskite or gold volume, V_j. Total transmittance (T) and total reflectance (R) are also calculated. High density mesh is considered in order to achieve better accuracy and ensure the convergence of the results, the minimum mesh refinement, 0.2 nm, being used in cubic volumes comprising gold nanoparticles. Our calculations are further validated by comparing the results obtained for the total absorptance, estimated through $A = 1 - R - T$, with those calculated numerically as $A = A_P + A_{Au}$. We consider as a reference system a perovskite slab without AuNPs. Calculations of T_{Ref}, R_{Ref}, and A_{Ref} realized

by means of an analytical model based on refraction and transmission coefficients in plane-parallel systems are compared to numerical ones.

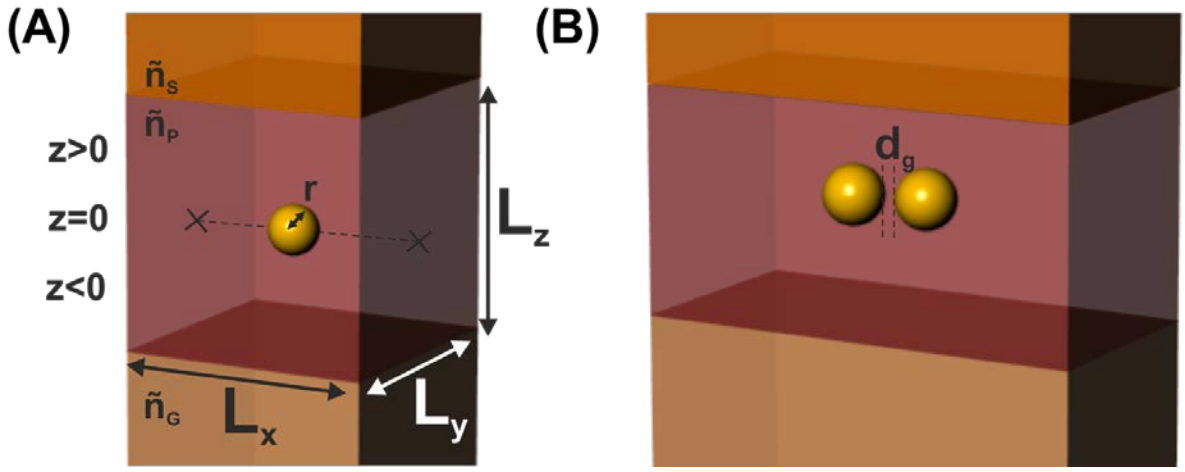

Figure 1. (A) Schematics of a unit cell with dimensions $L_x \times L_y \times L_z$, of a glass-perovskite-SpiroOMeTAD system, each layer characterized with refractive indexes, $\tilde{n}_G(\omega)$, $\tilde{n}_P(\omega)$ and $\tilde{n}_S(\omega)$ respectively, containing a gold nanoparticle (AuNP) of radius r centered at $(x, y, z = 0,0,0)$ nm. (B) Schematics of the same system as that in panel (A) containing 2 AuNPs with a gap distance d_g in a double volume $2 \cdot (L_x \times L_y \times L_z)$.

The solar absorptance enhancement of the perovskite film, η, is determined by:

$$\eta = \frac{\int_{400}^{775} A_P(\lambda) \cdot \mathrm{AM1.5} d\lambda}{\int_{400}^{775} A_{Ref}(\lambda) \cdot \mathrm{AM1.5} d\lambda}$$

with AM1.5 the normalized solar spectrum at the Earth surface with units [Photons·m^{-2}·s^{-1}· nm^{-1}].[26] With this definition, η > 1 implies an absorption enhancement, that is, the inclusion of AuNPs is beneficial for increasing the perovskite absorptance, and η < 1 indicates a detrimental effect of perovskite absorptance. In the calculations, the upper limit of the integral is taken to be

775 nm, as it has been demonstrated[20,27] that perovskite absorptance at larger wavelengths does not lead to an increment of the external quantum efficiency (EQE). Therefore, we will limit our calculations to the integration range [400,775] nm. The set of geometrical parameters defining the perovskite volume ($V_P = L_x \times L_y \times L_z$), and sphere size (of radius r) is chosen according to experimental realization.[20,27] In particular, we analyze the effect caused in the perovskite absorptance by embedding AuNPs as a function of: *particle size*, by changing the radius of the sphere; *concentration*, by modifying the surrounding perovskite volume; *particle location* inside the perovskite film; and *dimer formation*.

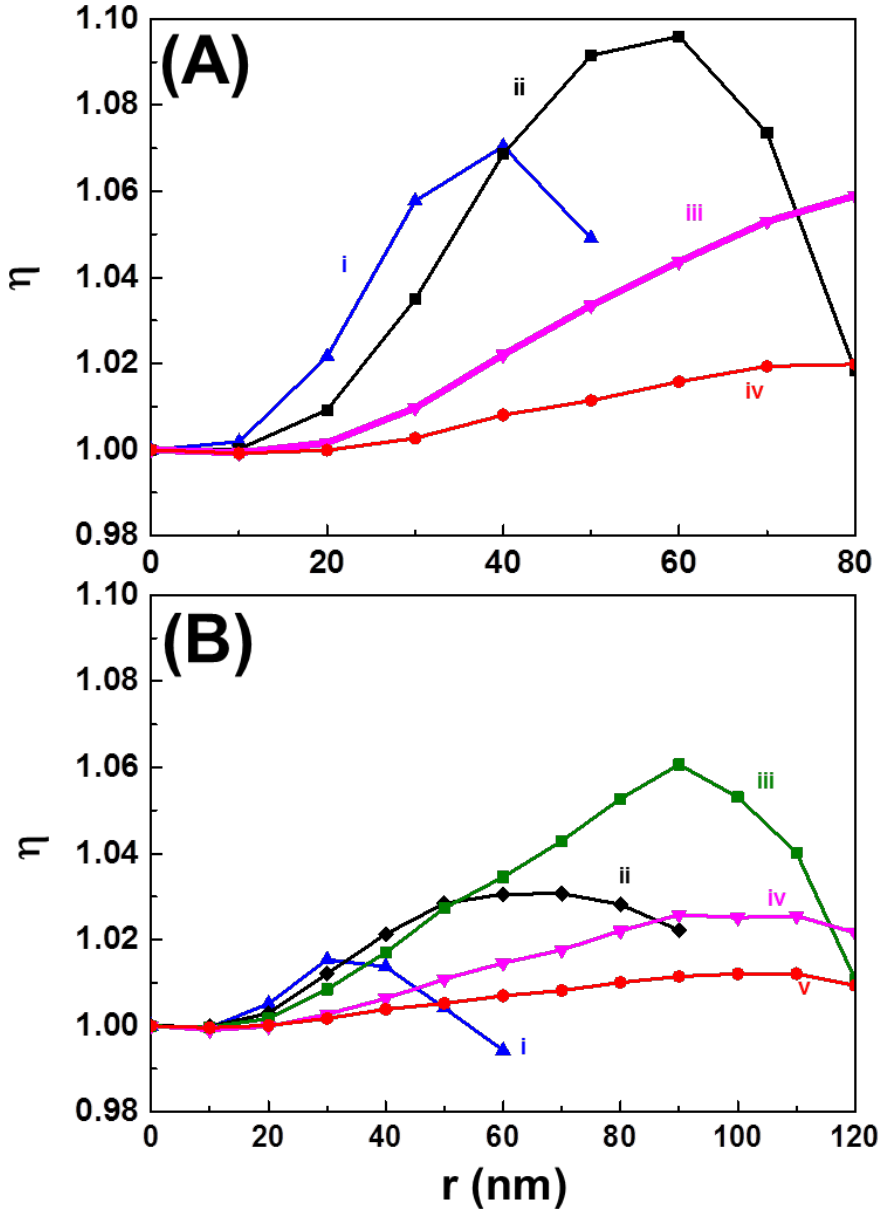

Figure 2. Perovskite solar absorption enhancement, η, as a function of the AuNP radius, r, in a glass-perovskite-SpiroOMeTAD system with $L_x = L_y$. In panel (A) it is taken L_z = 200 nm with L_x (i) 125 nm, (ii) 200 nm, (iii) 400 nm, and (iv) 600 nm; and in panel (B) L_z = 300 nm, taking L_x (i) 150 nm, (ii) 225 nm, (iii) 300 nm, (iv) 450 nm, and (v) 600 nm.

Figure 2 shows the perovskite solar absorptance enhancement, η, as a function of NP radius, r, for different concentrations, i.e., different perovskite volumes $L_x \times L_y \times L_z$ (as indicated in the figure), with (A) L_z = 200 nm, and (B) L_z = 300 nm (Figure S2 in the Supporting Information shows results also for L_z = 100 nm systems). A general trend is observed in all cases: η increases with particle radius until it gets to a maximum. In particular, we find the largest enhancement for (A) AuNPs of 60 nm radius in a 200×200×200 nm^3 perovskite volume, and for (B) AuNPs of 90 nm radius in a 300×300×300 nm^3 perovskite volume, which in both cases correspond to a filling fraction (V_{Au}/V_P) of 11.3% (corresponding filling fraction values of all the other cases here considered appear in Table S1 and Table S2 in the Supporting Information). At this stage, plasmonic coupling was prevented by considering long enough separation distances between neighboring gold particles. This was confirmed by simulations of field enhancement in systems of $2L_x \times 2L_y \times L_z$ containing 2 spheres separated a distance $(L_x - 2r)$ and $(L_y - 2r)$ along the corresponding directions. These systems would correspond to an equivalent system whose unit cell contains 2 unit cells of those considered for single spheres in a V_P volume. Modeled field enhancement and scattering effects, as well as the resulting absorption profiles, do not show any difference when compared to those observed for individual particles (Figure S3 in the Supporting Information). Hence, absorptance enhancements reported in Figure 2 can be considered as exclusively due to the presence of isolated spheres, and not to array effects.

For the case of L_z = 300 nm, absorptance spectra of perovskite and gold are displayed in Figure 3A and 3B, respectively, for several NP radius. For comparison, we also show results obtained for the reference system, that is, the corresponding perovskite volume without any AuNP, which has been calculated with both FDTD and semi-analytical models. As expected, the presence of a AuNP has a strong impact on the perovskite absorptance at long visible wavelengths. In panel

(A) we observe that for all particle sizes, absorption of light by the methyl ammonium lead iodide perovskite material decreases for wavelengths shorter than 500 nm as the particle radius increases. However, for $\lambda \geq$ 500 nm, the perovskite absorptance increases for all sizes, a maximum being found for r = 90 nm. In panel (B), where only the light captured by the metal is considered, the shape of the absorptance curve demonstrates that the amount of light captured by the metal continuously increases with particle size at all wavelengths. Interestingly, competition between these two absorbing materials results in larger absorptance of gold only at very short and long wavelengths, hence the typical absorptance spectra of gold nanoparticles displaying plasmon resonances at $\lambda\sim$ 550 nm are not observed. This is a direct consequence of considering a strongly absorbing host medium surrounding the gold particle. However, in systems with less perovskite volume, competition between both materials is more balanced and plasmonic resonances are apparent, as shown in Figure S4 in the Supporting Information for the case of L_z = 200 nm. In this case in which the perovskite slab absorbs less as a whole due to the lower amount of material, absorption of gold displays a plasmon resonance at $\sim$ 600 nm (the redshift arising due to the large real part of the refractive index of the external medium) which increases in intensity with the sphere radius. Contour plots in Figure 3 display (from top to bottom) the absorption profile at $\lambda =$ 450 nm, $\lambda =$ 600 nm, and $\lambda =$ 750 nm (maximum absorptance), respectively, for a AuNP of r = 90 nm. Analysis of the results at $\lambda =$ 750 nm reveal that a double contribution from near field and scattering effects caused by the presence of plasmonic NPs in the perovskite film leads to reinforced light harvesting by the semiconductor. Contrarily, at those wavelengths for which the magnitude of scattering significantly overcomes that of near field localization, the enhancement effect is substantially less noticeable or even absent. This consideration is of utmost importance for the potential use of metal particles as light harvesting

enhancers in optoelectronic devices. Previous plasmonic particle based approaches aiming at enhancing absorptance in perovskite solar cells usually consider silica coated AuNPs[22,28], thus suppressing near optical field effects which, as we herein demonstrate, would have been essential to actually improve the productive absorption of the cell. Our results are also in agreement with previous works,[22] in which no absorption enhancement was observed for particle sizes of $r \approx 20$ nm. The relative contribution of the two main effects affecting perovskite absorption, i.e., scattering and near field localization, will vary significantly depending on the thickness of the slab considered. Moreover, results will also depend on particle size not only because of the volume it occupies at the expense of perovskite material, but also for the reason that plasmonic near field and light scattering effects have a strong dependence on the sphere diameter. All these considerations explain why maxima in Figure 2 are found at different particle sizes and concentrations as a function of slab thickness.

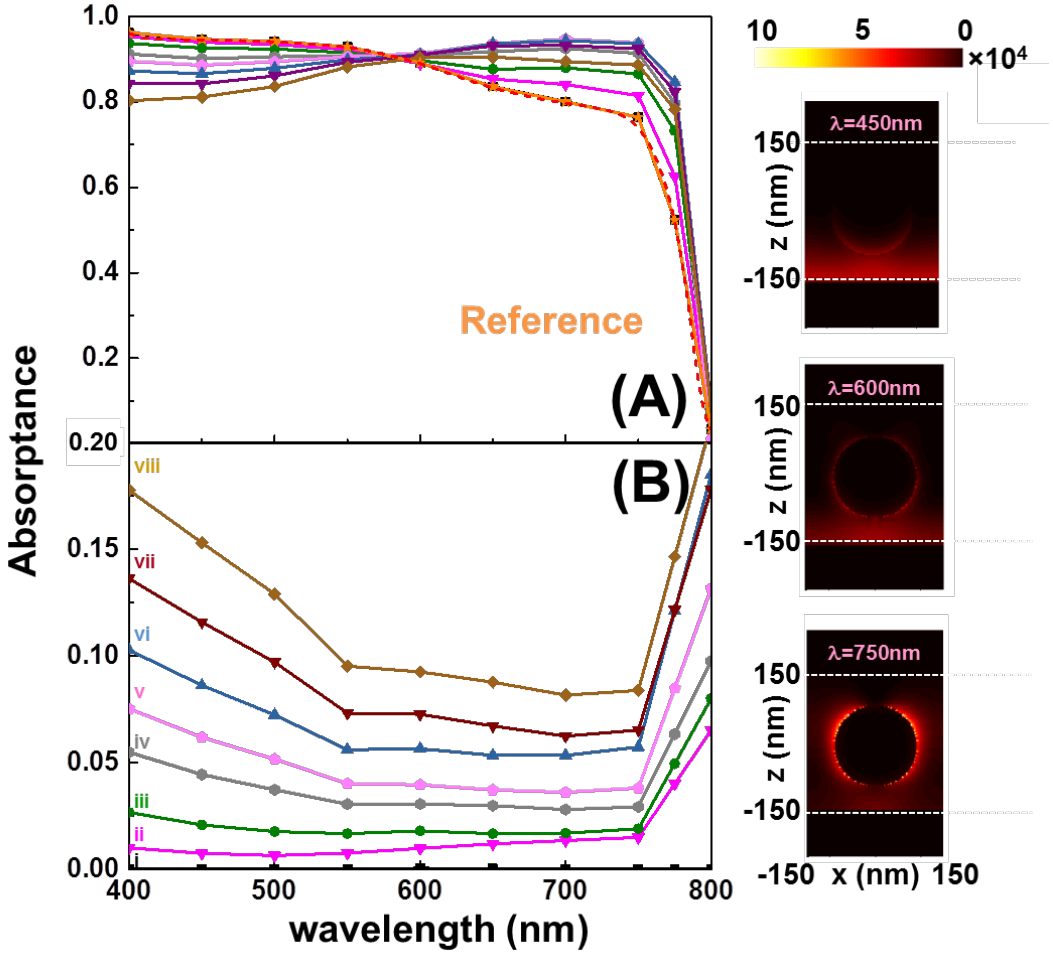

Figure 3. Absorptance spectra of a 300×300×300 nm^3 perovskite slab with AuNPs (r = 90 nm) inside, for several sphere radius ((i) 10 nm, (ii) 40 nm, (iii) 60 nm, (iv) 80 nm, (v) 90 nm, (vi) 100 nm, (vii) 110 nm, (viii) 120 nm). Panel (A) displays absorption of perovskite, and panel (B) of gold. Contour plots on the right correspond to absorption profiles at λ = 450 nm, 600 nm and 750 nm (from top to the bottom) for a 90 nm radius AuNP.

In what follows, we analyze the effect on the optical response of the slab of other features which are likely to be present in a dispersion of metal particles in a solid film, i.e., random particle location inside the perovskite slab and formation of dimers. The former is analyzed by considering different particle locations along the z-direction inside the slab. In Figure 4 we analyze in detail those cases for which we found maximum perovskite solar absorptance enhancement in Figure 2 (i.e, L_z = 200 nm and r = 60 nm; and L_z = 300 nm and r = 90 nm). Panel (A) shows η as a function of particle position along the z-direction. Note that z = 0 nm corresponds to a particle centered inside the slab, $z < 0$ nm to systems in which the particle is located close to the glass substrate (that is, close to the illumination source), and $z > 0$ nm to cases in which the particle is closer to the spiro-OMeTAD cover (far from the illumination source). Circles represent results for perovskite slabs of thickness L_z = 200 nm with embedded gold spheres of r = 60 nm, while squares stand for L_z = 300 nm containing spheres of r = 90 nm. Dashed lines display the expected average enhancement assuming a random metal particle distribution within the semiconductor film for L_z = 200 nm and L_z = 300 nm, respectively. For L_z = 200 nm, a maximum enhancement is found for spheres located at z = +20 nm (far from the source) leading to an enhancement of ~ 12%, while for thicker films the maximum enhancement (~ 6%) is obtained at z = -10 nm. This means that light must travel ~ 50 nm within the perovskite film before it reaches the plasmonic scatterer in order to obtain an optimum performance. In addition, these results demonstrate that random distribution of particles along the z-direction will lead to average enhancements of ~ 7% and 5% for L_z = 200 nm and L_z = 300 nm, respectively. Panel (B) displays absorptance spectra for a L_z = 300 nm unit cell containing a AuNP of r = 90 nm at different z positions (z = -50 nm, z = -10 nm, and z = 50 nm), whose comparison shows that the shape of the curve is very sensitive to this parameter. Contour plot

insets correspond to absorption profiles at $\lambda = 750$ nm, the wavelength at which maximum absorptance is found. From them, we can conclude that near field effects dominate when the particle is close to the substrate, while scattering effects do when it is located near the spiro-OMeTAD cover. It is precisely the double contribution of plasmonic near field and scattering effects found when the particle is closer to the center of the slab what leads to a maximum enhancement of the perovskite absorptance. Corresponding results for a L_z = 200 nm slab are shown in Figure S5 in the Supporting Information.

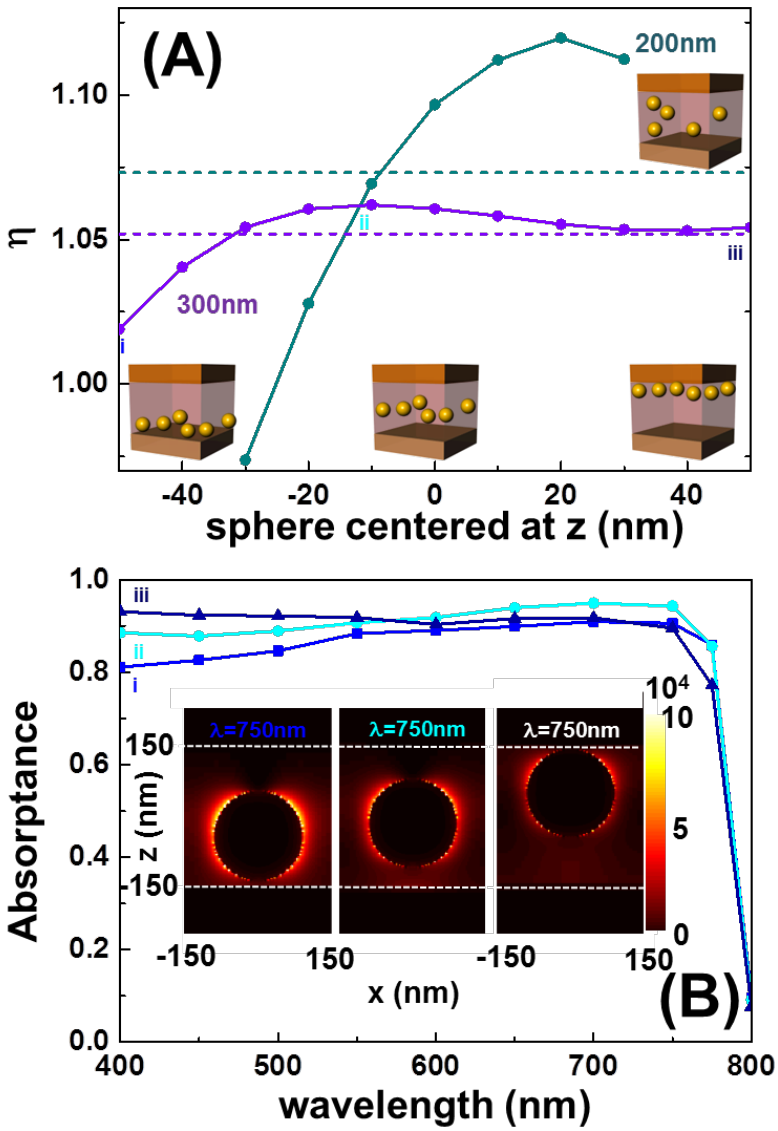

Figure 4. (A) Perovskite solar absorption enhancement, η, as a function of the z position of the AuNP inside the perovskite slab. Circles account for a 200×200×200 nm^3 system with a sphere of r = 60 nm, and squares for a 300×300×300 nm^3 with a sphere of r = 90 nm. Dashed lines correspond to the average value for all z positions in each case. (B) For the 300×300×300 nm^3 case, absorptance spectra at several z positions, (i) z = -50 nm, (ii) z = -10 nm, and (iii) z = +50 nm. Colours correspond to the positions indicated in panel (A). The inset displays corresponding absorption profile at λ = 750 nm.

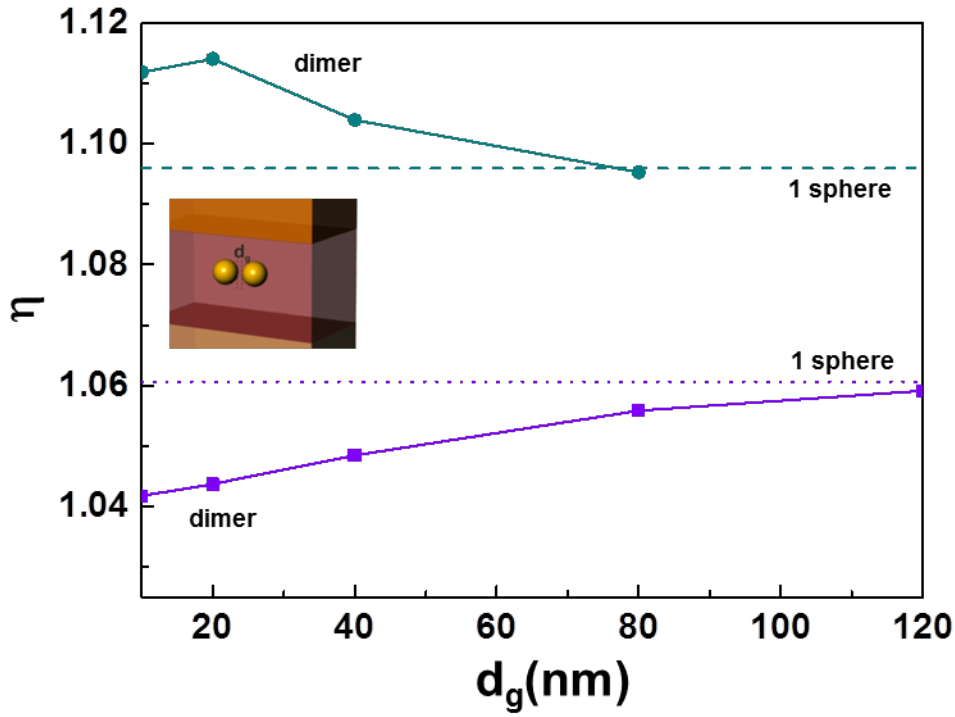

Figure 5. (A) Perovskite solar absorption enhancement, η, as a function of the gap distance, d_g, between 2 AuNPs of (i**)** 60 nm radius in a 200×400×200 nm^3 system (circles), and (ii) 90 nm radius in a 300×600×300 nm^3 system (squares). Horizontal dashed and dotted lines correspond to η of single spheres of the same radius in half volumes, correspondingly.

Although we are dealing with diluted solid suspensions of the metal particles in perovskite, formation of dimers during the actual preparation of the films cannot be entirely discarded. Thus the analysis of the optical effects of this eventual outcome is also needed. For this reason, in Figure 5 we analyze the effect of dimer formation in perovskite films keeping the same concentration as before, i.e., considering 2 AuNPs in a double volume of $2(L_x \times L_y \times L_z)$ of perovskite. Panel (A) in Figure 5 displays perovskite solar absorptance enhancement as a

function of the gap between the two particles, d_g, for perovskite volumes of 200×400×200 nm^3 containing 2 spheres of r = 60 nm (circles), and of 300×600×300 nm^3 containing 2 spheres of r = 90 nm (squares). Interestingly, formation of dimers is decidedly beneficial for thin perovskite slabs (in comparison to results for 1 AuNP), reaching a highest enhancement of almost 12% for gap distances of 20 nm, but the opposite effect is obtained for thicker films. For comparison, dashed and dotted lines represent the corresponding absorptance enhancement of a single sphere in half a volume (200× 200×200 nm^3 and 300×300×300 nm^3, respectively). In both cases, as d_g approaches the separation distance of an equivalent system comprising 2 unit cells with 1 sphere per cell, the observed enhancement becomes that of a single sphere in half a volume, further confirming that array effects are excluded in our simulations. The different effect of dimers on the absorption of each slab thickness herein considered has its origin in the dissimilar response of both perovskite films at long wavelengths. This can be clearly seen in Figure 6, where we plot reflectance, transmittance and absorptance for the case of the presence of dimers as well as that of single spheres in the two types of films. For the systems here considered and d_g = 10 nm we find that dimers scatter light mostly in the forward direction for the L_z = 300 nm case, which gives rise to a much higher transmittance in comparison with single spheres, while for the L_z = 200 nm case, the opposite behavior is found, i.e., higher transmission is found for single spheres in comparison to dimers. Corresponding field enhancement and absorption profiles at the wavelength at which perovskite absorptance is maximum are shown in Figures S6 and S7 in the Supporting Information, where it can be seen that the hot spot created in the interparticle gap occupies such a small volume that the effect on the perovskite absorptance is much less significant than that of scattering.

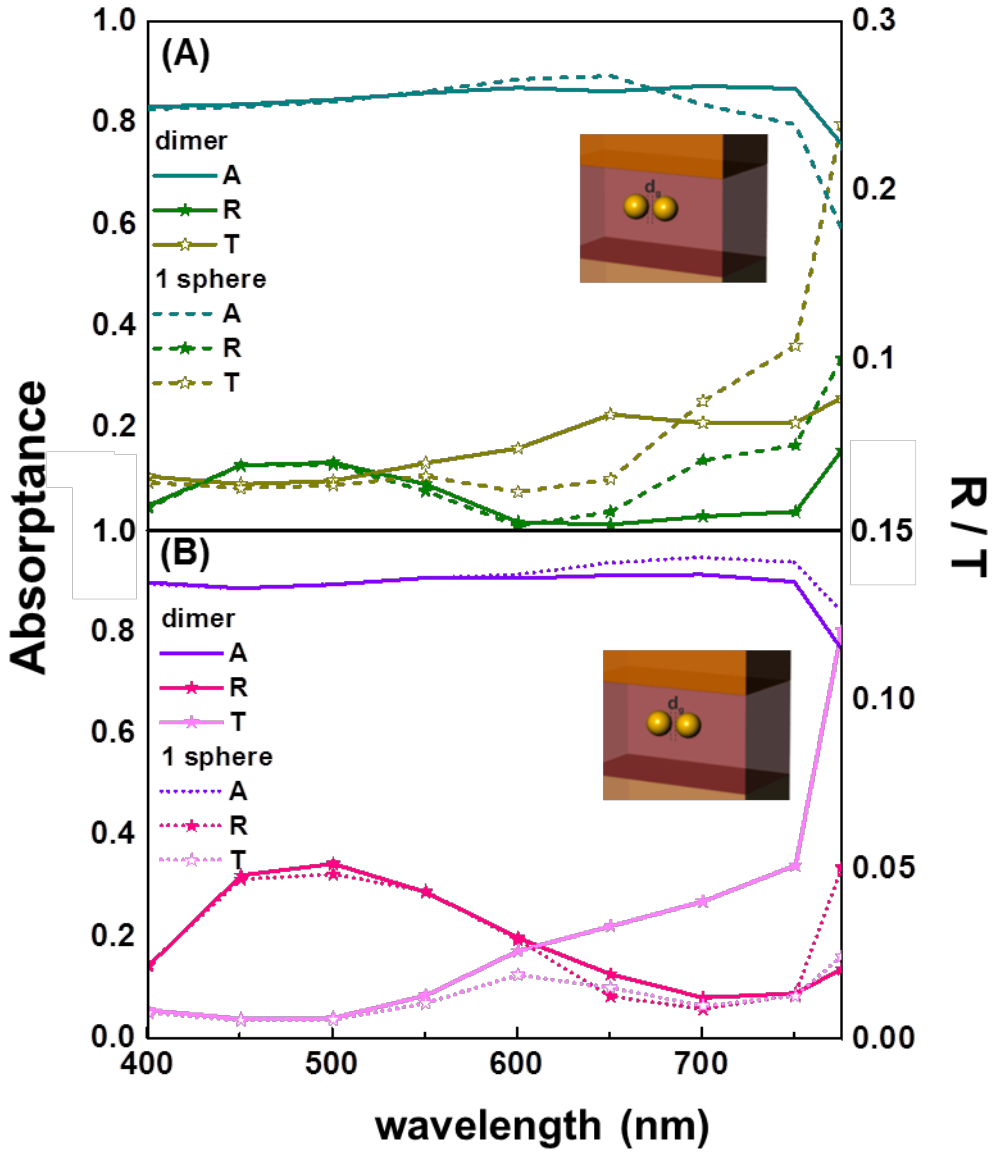

Figure 6. Reflectance, transmittance and perovskite absorptance spectra for single spheres (discontinuous lines) and dimers with gap distances of 10 nm (solid lines) of (A) 60 nm radius in 200×400×200 nm^3 volumes and (B) 90 nm radius in 300×600×300 nm^3 systems, respectively.

CONCLUSIONS

In conclusion, we have demonstrated, by means of numerical simulations, that the inclusion of plasmonic gold nanoparticles in thin organic-inorganic halide perovskite films leads to an enhancement of perovskite sunlight absorption that ranges between 6% and 12% for the set of film thicknesses considered. We find specific sets of realistic parameters in terms of particle size and concentration to maximize perovskite absorption. We demonstrate that absorption is maximized when plasmonic near field and light scattering effects are adequately balanced. We have also analyzed the effect of having a random distribution of particles within the film, as well as the eventual formation of dimers, the conditions under which these events are beneficial or detrimental for perovskite absorption being found. Our results provide a guide to find the best optical design based on plasmonic effects for standard composition and thickness perovskite films, and open the door to performance optimization of perovskite solar cells by the inclusion of gold nanoparticles within the active layer.

ASSOCIATED CONTENT

Supporting Information. Figures providing perovskite solar absorptance enhancement for L_z = 100 nm film thickness, field enhancement and absorption profiles for single spheres at several locations inside perovskite films of L_z = 200 nm, and results for dimers. This material is available free of charge via the Internet at http://pubs.acs.org.

AUTHOR INFORMATION

Corresponding Author

*Email: h.miguez@csic.es

Notes

The authors declare no competing financial interests.

ACKNOWLEDGMENT

Financial support of the European Research Council under the European Union's Seventh Framework Programme (FP7/2007−2013)/ERC grant agreement n° 307081 (POLIGHT) and the Spanish Ministry of Economy and Competitiveness under grant MAT2014-54852-R, is gratefully acknowledged.

REFERENCES

(1) Lee, M. M.; Teuscher, J.; Miyasaka, T.; Murakami, T. N.; Snaith, H. J. Efficient Hybrid Solar Cells Based on Meso-Superstructured Organometal Halide Perovskites. *Science* **2012**, 338, 643.

(2) Green, M. A.; Ho-Baillie, A.; Snaith, H. J. The emergence of perovskite solar cells. *Nat. Photonics* **2014**, 8, 506−514.

(3) Burschka, J.; Pellet, N.; Moon, S-J.; Humphry-Baker, R.; Gao, P.; Nazeeruddin, M. K.; Grätzel, M. Sequential deposition as a route to high-performance perovskite-sensitized solar cells. *Nature* **2013** 499, 316–319.

(4) Liu, M.; Johnston, M. B.; Snaith, H. J. Efficient planar heterojunction perovskite solar cells by vapour deposition. *Nature* **2013** 501, 395–398.

(5) Xiao, M.; Huang, F.; Huang, W.; Dkhissi, Y.; Zhu, Y.; Etheridge, J.; Gray-Weale, A.; Bach, U.; Cheng, Y-B.; Spiccia, L. A Fast Deposition-Crystallization Procedure for Highly Efficient Lead Iodide Perovskite Thin-Film Solar Cells. *Angew. Chem. Int. Ed.* **2014**, 53, 9898 –9903.

(6) Jeon, N. J.; Noh, J. H.; Kim, Y. C.; Yang, W. S.; Ryu, S. Solvent engineering for high-performance inorganic–organic hybrid perovskite solar cells. *Nat. Materials* **2014**, 13, 897–903.

(7) Nie, W.; Tsai, H.; Asadpour, R.; Blancon, J-C.; Neukirch, A. J.; Gupta, G.; Crochet, J. J.; Chhowalla, M.; Tretiak, S.; Alam, M. A.; Wang, H-L.; Mohite, A. D. High-efficiency solution-processed perovskite solar cells with millimeter-scale grains. *Science* **2015**, 347, 6221.

(8) Eperon, G. E.; Stranks, S. D.; Menelaou, C.; Johnston, M. B.; Herza, L. M.; Snaith, H. J. Formamidinium lead trihalide: a broadly tunable perovskite for efficient planar heterojunction solar cells. *Energy Environ. Sci.*, **2014**,7, 982-988.

(9) Roldán-Carmona, C.; Malinkiewicz, O.; Soriano, A.; Mínguez Espallargas, G.; Garcia, A.; Reinecke, P.; Kroyer, T.; Ibrahim Dar, M.; Khaja Nazeeruddin, M.; Bolink. H. J. Flexible high efficiency perovskite solar cells. *Energy Environ. Sci.*, **2014**, 7, 994-997.

(10) Noh, J. H.; Im, S. H.; Heo, J. H.; Mandal, T. N.; Seok, S. I. Chemical Management for Colorful, Efficient, and Stable Inorganic–Organic Hybrid Nanostructured Solar Cells. *Nano Lett*. **2013**, 13, 1764−1769.

(11) Hao, F.; Stoumpos, C. C.; Cao, D. H.; Chang, R. P. H.; Kanatzidis, M. GLead-free solid-state organic–inorganic halide perovskite solar cells. *Nat. Photonics* **2014**, 8, 489–494.

(12) Noel, N. K.; Stranks, S. D.; Abate, A.; Wehrenfennig, C.; Guarnera, S.; Haghighirad, A-A.; Sadhanala, A.; Eperon, G. E.; Pathak, S. K.; Johnston, M. B.; Petrozza, A.; Herza, L. M.; Snaith, H. J. Lead-free organic–inorganic tin halide perovskites for photovoltaic applications. *Energy Environ. Sci*., **2014**, 7, 3061

(13) Anaya, M.; Lozano, G.; Calvo, M. E.; Zhang, W.; Johnston, M. B.; Snaith, H. J.; Míguez, H. Optical Description of Mesostructured Organic−Inorganic Halide Perovskite Solar Cells. *J. Phys. Chem. Lett.* **2015**, 6, 48−53.

(14) Lin, Q.; Armin, A.; Nagiri, R. C. R.; Burn, P. L.; Meredith, P. Electro-Optics of Perovskite Solar Cells. *Nat. Photonics* 2015, 9, 106–112.

(15) Ball, J. M.; Stranks, S. D.; Hö rantner, M. T.; Hüttner, S.; Zhang, W.; Crossland, E. J. W.; Ramirez, I.; Moritz, R.; Johnston, M. B.; Friend, R. H.; Snaith, H. J. Optical Properties and Limiting Photocurrent of Thin-Film Perovskite Solar Cells. *Energy Environ. Sci*. **2015**, 8, 602-609.

(16) Nishimura, S.; Abrams, N.; Lewis, B. A.; Halaoui, L. I.; Mallouk, T. E.; Benkstein, K. D.; Lagemaat, J. V.; Frank, A. Standing Wave Enhancement of Red Absorbance and Photocurrent in Dye-Sensitized Titanium Dioxide Photoelectrodes Coupled to Photonic Crystals. *J. Am. Chem. Soc*., **2003**, 125, 6306-6310.

(17) Colodrero, S.; Mihi, A.; Haggman, L.; Ocana, M.; Boschloo, G.; Hagfeldt, A.; Míguez, H. Porous One-Dimensional Photonic Crystals Improve the Power-Conversion Efficiency of Dye-Sensitized Solar Cells. *Advanced Materials*, **2009**, 21 (7), 764.

(18) López-López, C.; Colodrero, S.; Míguez, H. Panchromatic porous specular back reflectors for efficient transparent dye solar cells. *Phys. Chem. Chem. Phys*. **2014**, 16 (2), 663-668.

(19) Guldin, S.; Huttner, S.; Kolle, M.; Welland, M. E.; Muller-Buschbaum, P.; Friend, R. H.; Steiner, U.; Tétreault, N. Dye-sensitized solar cell based on a three-dimensional photonic crystal. *Nano Lett.* **2010**, 10 (7), 2303-2309.

(20) Zhang, W.; Anaya, M.; Lozano, G.; Calvo, M. E.; Johnston, M. B.; Míguez, H.; Snaith, H. J. Highly Efficient Perovskite Solar Cells with Tunable Structural Color. *Nano Lett.* **2015**, 15, 1698−1702.

(21) Myroshnychenko, V.; Rodriguez-Fernandez, J.; Pastoriza-Santos, I.; Funston, A. M.; Novo, C.; Mulvaney, P.; Liz-Marzan, L. M.; de Abajo, F. J. G. *Chem. Soc. Rev*. **2008**, 37, 1792.

(22) Zhang, W.; Saliba, M.; Stranks, S. D.; Sun, Y.; Shi, X.; Wiesner, U.; Snaith, H. J. Enhancement of Perovskite-Based Solar Cells Employing Core–Shell Metal Nanoparticles. *Nano Lett.*, **2013**, *13* (9), pp 4505–4510

(23) Zelin Lu, Xujie Pan, Yingzhuang Ma,Yu Li, Lingling Zheng, Danfei Zhang, Qi Xu, Zhijian Chen, Shufeng Wang, Bo Qu, Fang Liu, Yidong Huang, Lixin Xiao and Qihuang Gong. Plasmonic-enhanced perovskite solar cells using alloy popcorn nanoparticles. *RSC Adv*. **2015**, *5*, 11175-11179.

(24) Hsua, H-L.; Juang, T-Y.; Chenc, C-P.; Hsieh, C-M.; Yang, C-C.; Huang, C-L.; Jenga, R. J. Enhanced efficiency of organic and perovskite photovoltaics from shape-dependent broadband plasmonic effects of silver nanoplates. *Sol. Energ. Mat. Sol. Cells.* **2015**,140, 224–231.

(25) Johnson, P. B.; Christy, R. W. Optical Constants of the Noble Metals. *Phys. Rev. B* **1972**, *6, 12, 4370-4379.*

(26) http://rredc.nrel.gov/solar/spectra/am1.5/

(27) Burschka, J.; Pellet, N.; Moon, S-J.; Humphry-Baker, R.; Gao, P.; Nazeeruddin, M. K.; Grätzel, M. Sequential deposition as a route to high-performance perovskite-sensitized solar cells. *Nature* **2013**,*499, 316–319.*

(28) Spinelli, P.; Polman, A. Prospects of near-field plasmonic absorption enhancement in semiconductor materials using embedded Ag nanoparticles. *Optics Express* **2012** *20, S5, A642*